

Advanced Reservoir Imaging Using Frequency-Dependent Seismic Attributes

Type of Report: Final
Reporting Period Start Date: January 1, 2005
Reporting Period End Date: December 31, 2007

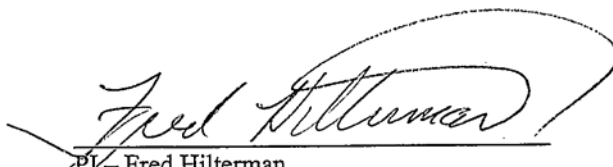
Principal Authors:

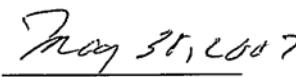
PI - Fred Hilterman – Professor, University of Houston, Houston, TX
Co-PI – Tad Patzek – Professor, University of California, Berkeley, CA
Gennady Goloshubin – Research Professor – University of Houston, TX
Dmitriy Silin – Associate Researcher – University of California, Berkeley, CA,
Charlotte Sullivan – Research Assistant Professor, University of Houston, Houston, TX
Valeri Korneev, Staff Scientist, LBNL, Berkeley, CA.

DOE Award Number: DE-FC26-04NT15503 [Subsurface Imaging]
Submitting Organizations:

Department of Geosciences
University of Houston
Houston, Texas 77204-5505

Civil and Environmental Engineering
210 Ericsson Building, MC 1716
University of California
Berkeley, CA 94720-1716


PI - Fred Hilterman
Professor
University of Houston


Date

ABSTRACT

Our report concerning advanced imaging and interpretation technology includes the development of theory, the implementation of laboratory experiments and the verification of results using field data. We investigated a reflectivity model for porous fluid-saturated reservoirs and demonstrated that the frequency-dependent component of the reflection coefficient is asymptotically proportional to the reservoir fluid mobility. We also analyzed seismic data using different azimuths and offsets over physical models of fractures filled with air and water. By comparing our physical model synthetics to numerical data we have identified several diagnostic indicators for quantifying the fractures. Finally, we developed reflectivity transforms for predicting pore fluid and lithology using rock-property statistics from 500 reservoirs in both the shelf and deep-water Gulf of Mexico. With these transforms and seismic AVO gathers across the prospect and its down-dip water-equivalent reservoir, fluid saturation can be estimated without a calibration well that ties the seismic. Our research provides the important additional mechanisms to recognize, delineate, and validate new hydrocarbon reserves and assist in the development of producing fields.

DISCLAIMER

This report was prepared as an account of work sponsored by an agency of the United States Government. Neither the United States Government nor any agency thereof, nor any of their employees, makes any warranty, express or implied, or assumes any legal liability or responsibility for the accuracy, completeness, or usefulness of any information, apparatus, product, or process disclosed, or represents that its use would not infringe privately owned rights. Reference herein to any specific commercial product, process, or service by trade name, trademark, manufacturer, or otherwise does not necessarily constitute or imply its endorsement, recommendation, or favoring by the United States Government or any agency thereof. The views and opinions of authors expressed herein do not necessarily state or reflect those of the United States Government or any agency thereof.

TABLE OF CONTENTS

TITLE PAGE	1
ABSTRACT.....	2
DISCLAIMER	3
TABLE OF CONTENTS.....	4
EXECUTIVE SUMMARY	5
INTRODUCTION	7
1. WAVE THEORY DEVELOPMENT.....	8
1.1. Reservoir Reflectivity	9
1.2 Amplitude versus offset & frequency	15
2. PHYSICAL MODELING.....	19
2.1. Experiment Set-Up and Data Acquisition.....	19
2.2. Amplitude vs. Azimuth	25
3. THEORY VERIFICATION WITH FIELD DATA	27
3.1. Rock-Property Transforms	28
3.2. Amplitude vs. Frequency	30
3.3. Amplitude vs. Offset and Frequency	32
CONCLUSIONS.....	34
TECHNOLOGY TRANSFER.....	35
REFERENCES	35
FUNDING.....	37

EXECUTIVE SUMMARY

Our report for an advanced imaging and interpretation technology includes *development of theory and processing algorithms, laboratory experiments and the verification of results using field data provided by industrial partners.*

During the reporting period the project focused on the following tasks:

1. Theoretical development

- Development of an asymptotic model and governing equations describing seismic wave propagation in fluid-saturated dual-porosity media. Investigation the interaction between the solid skeleton and the fluid at the transition between permeable zones.
- Description of reflectivity equations, development of algorithms and computer codes for numerical modeling of frequency-dependent seismic response for porous permeable layered medium.
- Development of frequency-preserved target-oriented seismic migration and algorithms for frequency-dependent AVO analysis.

2. Physical modeling

- Construction and utilization of the 3D anisotropic fractured physical model for investigation of wave attenuation within fractured material and azimuth- and frequency-dependent reflectivity of the porous model surfaces.
- Analyses of the physical modeling data with wide frequency band (10-300 kHz) for different azimuths and offsets over the model filled with air and water. Comparison of the numerical modeling result with the physical modeling data.

3. Field data processing

- Reprocessing of the existing seismic data with preserved amplitudes and frequencies. Estimation of seismic attributes.
- Construction of the reservoir geologic models of reservoir and calibration of the seismic attributes against the geologic models and reservoir parameters determined from well data.

We have developed the equations describing seismic wave propagation in dual porosity media and the low frequency asymptotic solution of the reflectivity for such media. We have evolved a methodology to determine the reservoir properties using the frequency-dependent reflectivity at different incident angles.

We have developed algorithms for preserving the wavelet frequency content and applied the low-frequency asymptotic approach to derive algorithms for reflection/transmission coefficients and attenuation that are dependent on frequency and fluid mobility.

Physical modeling is one technique we were employing to investigate wave propagation in fractured media. We have analyzed the physical modeling data for different azimuths and offsets over the model filled with air and water and compared the results of the

analysis with numerical modeling. Several diagnostic methodologies for evaluating of fractures were identified. The methodologies involved head waves and reflections.

We have described the structural and stratigraphic interpretation of various seismic volumes. We have formulated and developed rock-property transforms that allow conventional seismic horizon maps to be converted into reflectivity maps. These transforms were derived from rock-property trends of 500 reservoirs in both the shelf and deep-water Gulf of Mexico. With these transforms and the AVO gathers at the prospect and at the down-dip water-equivalent reservoir, a fluid saturation can be estimated without a calibration well that ties the seismic unless the bed thickness is desired.

We have developed a spectrum cross-plot technique based on AVO & Frequency analyses and applied this technique to separate wet- and gas-saturated zones.

The results of the investigations will help to find new hydrocarbon prospects in areas that have subtle to no seismic expression, and these prospects are deeper and more costly to find and drill. The analysis of frequency-dependent AVO attributes and low-frequency imaging leads to accurate predictions of pore-fluid production by mapping fluid contacts and fluid mobility. This represents a major step in the goal of developing a seismic-based method of reservoir permeability mapping. The research work provides the additional mechanism to recognize, delineate, and validate new hydrocarbon reserves and assist in the development of producing fields

INTRODUCTION

The project goal is to develop seismic-based technology that correlates and/or quantifies a reservoir's fluid-saturation properties and their spatial distribution to frequency- and angle-dependent reflectivity.

The DHI based on "bright-spot" recognition of hydrocarbons became routine during the 1970s. Shortly after, 3-D acquisition more accurately delineated the structure of bright-spot reservoirs. However, most large bright-spot reservoirs have been drilled. Energy companies are now drilling prospects in areas that have subtle to no seismic expression of hydrocarbons and these prospects are deeper and more costly to drill. Our work provides a mechanism of frequency-dependent reservoir reflectivity to recognize, delineate, validate new reserves and assist in the development of hydrocarbon fields.

We have worked for developing technologies that will assist in the recognition of hydrocarbon accumulations from 3-D seismic data and also providing technologies to predict reservoir rock type, pore-fluid properties and the delineation of hydrocarbon distribution. In addition, we anticipate the technologies will assist in the more complete and economic draining of the reservoir's hydrocarbons.

The project involves theory and processing-algorithm development, numerical and physical modeling, laboratory experiments and field verification using seismic, well-log and engineering data. Extensions to wave-equation models with fluid-flow in dual-porosity media and frequency-dependent analysis are two major theoretical developments.

Initial results from low seismic frequencies and/or far-offset data provided detailed images of hydrocarbon reservoirs not seen on conventional data. Many observations were not explained by elastic wave theory. We have provided simultaneous research using long-offset seismic data in the areas of non-elastic wave propagation with fluid flow, target-oriented processing and the development of geologic workflows for multi-trace seismic attributes. This multi-discipline study was the reason for the research collaboration between the Universities of Houston and California, Berkeley.

The Report contains three main sections. First, we briefly summarize our theoretical results. Then, the second section presents the principle results in physical modeling. The last one contains some results of processing and interpretation of field data. Publication material is presented in Appendixes.

1. WAVE THEORY DEVELOPMENT

Milestones

The milestones for wave-theory development:

- Asymptotic model and governing equations describing seismic wave propagation in dual-porosity media,
- Formulation of reflectivity equations, development of algorithms and computer codes for numerical modeling of frequency-dependent seismic imaging for porous permeable layered medium,
- Frequency preserving migration and algorithms for extracting frequency-dependent signal from seismic data,

Approach and Accomplishments:

We investigated the dependence of scaling on the dynamic Darcy's law relaxation time, which turns out to be linearly related to Biot's tortuosity parameter. The results are published in "Transport in porous media", 2006. We have developed theory of wave propagation in dual-porosity media. Our development combines Biot's poroelasticity theory, Barenblatt's dual porosity model of fluid flow in fractured rocks, and asymptotic analysis. Goloshubin and Silin have presented the development of the theory at the 2006 SEG meeting in New Orleans and at the 2006 EAGE Meeting in Vienna.

The coefficients of normal-incident reflection and transmission of a planar p-wave from a boundary between two layers in a fractured reservoir were studied in the low-frequency range. The coefficients are expressed as power series with respect to a small dimensionless parameter, which is a function of the reservoir fluid mobility. The simple asymptotic expressions for reflection and transmission coefficients provide new opportunities for seismic modeling and inversion. It also suggests new frequency-dependent attributes, proportional to the reservoir fluid mobility. The results on the asymptotic solutions will be presented at 2007 SEG Meeting in San Antonio (Goloshubin and Silin).

Amplitude-versus-offset (AVO) programs for generating offset source-receiver synthetics for isotropic and VTI anisotropic layered models have been developed and tested. The programs are based on ray theory and handle industry-standard well-log suites.

Several spectral decomposition programs were evaluated for estimating the low-frequency content of seismic field data and these were converted into DISCO (commercial software package) routines that are callable from our 3-D seismic processing package. We have tested our algorithms against published results and ours are more accurate for large source-receiver offsets. As a validation test, numerical modeling synthetics and physical modeling data have been processed with the frequency-preserving target-oriented migration algorithm for various dip angles and acquisition geometries. Amplitudes and spectra derived from the migrated synthetics closely match our theoretical predictions. The results on 3-D migration of the physical modeling data were presented at 2006 SEG Meeting in New Orleans (Chen, Hilterman, and Doruelo).

1.1. Reservoir Reflectivity

In case of porous fluid-saturated medium the poroelasticity theory (Biot, 1956) predicts a movement of the pore fluid relative to the skeleton for seismic wave propagation through the medium. This phenomenon opens an opportunity for investigating the flow properties of hydrocarbon-saturated reservoirs with seismic measuring. But, it is well known that relative fluid movement becomes negligible at low frequencies.

The presence of fractures or other high permeable channels has a significant impact on the flow properties of reservoir rocks. Two or more scales of permeability are usually observed. A connected system of fractures, due to relatively simple geometry of the pore space, is highly permeable for fluid flow. The matrix, due to the tortuous pores and pore throats, is significantly less permeable. At the same time, the total volume of the fractures (high permeable channels) is usually small and the matrix blocks contain most of the reservoir fluid. This contrast leads to the dual-medium model of reservoir rock, which was originally proposed by Barenblatt et al. (1960). According to this model, the fluid flow in matrix blocks is local: it only supports the exchange of fluid between individual blocks and the surrounding fractures. In large scale, fluid flows through the fractures only. In this study, we apply Barenblatt's approach to flow in fractured rocks. A combination of this approach with Biot's theory of elastic wave propagation in permeable porous media leads to a model, which we call Biot-Barenblatt poroelastic model. In fact, the applicability of this model is not limited to fractured rocks only. It is justified whenever the permeability of the rock has two or more contrasting scales. These scales must be distributed in the medium in such a way that every representative volume comprises both, a small-volume highly permeable medium and a low-permeable analog of matrix. Recent studies suggest that even in a "classical" porous rock, such as sandstone, the fluid flows through a very small portion of the pore space, while the majority part of it is in stagnation. Aside from the effect of fluid flow by means of the dual-medium model we have utilized the effects of scattering (Gurevich, et al., 1997) in case of finely-layered porous rocks. So, we have performed a numerical study of the reflectivity in case of finely-layered permeable reservoir, caused by both interlayer fluid flow and scattering.

Our main objective is to characterize the normal-incident P-wave reflection from the inhomogeneous layered reservoir with dual porosity and permeable boundaries between layers within this reservoir and to investigate the influence of different fluid saturation on the seismic reservoir response. It is a continuation of the previous study (Goloshubin and Silin, 2006), where reflection and transmission coefficients at the permeable boundary within a fractured reservoir have been investigated.

This paper is organized as follows. First, we extract a brief summary of asymptotic analysis of the reflection and transmission coefficients from a permeable boundary for the fast incident P-wave. Then we construct the formulas for calculation of the reservoir reflectivity and discuss some examples of the calculation of the frequency-dependent

reflection amplitudes from both homogeneous and inhomogeneous porous fluid-saturated layers.

Reflection from a permeable boundary

According to Biot (1956 a,b) a compressional P-wave in a fluid-saturated porous medium is a superposition of slow and fast waves. These two waves are always coupled and neither one can exist separate from the other. The same holds true in a fractured reservoir. The main difference is that in a dual-porosity medium, the permeability is decoupled from the porosity. The permeability of the system of fractures is governed by Darcy's law and is characterized by a coefficient of permeability, κ . Fluid flow in the matrix is local, limited to the exchange with the surrounding fractures.

Although the attenuation of the slow wave is high, we have to consider two coupled incident waves, fast and slow. Each of the two coupled incident waves, fast and slow, generates a pair of fast and slow reflected and transmitted waves. The superposition principle allows for considering each incident wave separately. We denote the respective transmission and reflection coefficients by T_{FF} , T_{FS} , R_{FF} , R_{FS} , etc. A double subscript denotes the type of incident and transmitted (or reflected) waves. For example, R_{FS} denotes the reflection coefficient corresponding to fast incident and slow reflected wave.

Based on mass and momentum conservation imply the following boundary conditions:

$$\begin{aligned} u_1 \Big|_{x=0} &= u_2 \Big|_{x=0} \\ W_1 \Big|_{x=0} &= W_2 \Big|_{x=0} \\ p_{f1} \Big|_{x=0} &= p_{f2} \Big|_{x=0} \\ \frac{1}{\beta_1} \frac{\partial u_1}{\partial x} \Big|_{x=0} &= \frac{1}{\beta_2} \frac{\partial u_2}{\partial x} \Big|_{x=0} \end{aligned}$$

Where u_j the displacement for the solid skeleton, W_j the Darcy velocity, p_{fj} the fluid pressure, and β_j the compressibility of the rocks above ($j=1$) and below ($j=2$) a permeable boundary.

The following asymptotic results have been obtained for the first incident wave in a dimensionless form (Goloshubin and Silin, 2006)

$$\begin{aligned} R_{FF} &= R_{FF}^0 + R_{FF}^1 \sqrt{\varepsilon} + O(|\varepsilon|) \\ T_{FF} &= T_{FF}^0 + T_{FF}^1 \sqrt{\varepsilon} + O(|\varepsilon|) \\ R_{FS} &= R_{FS}^1 \sqrt{\varepsilon} + O(|\varepsilon|) \\ T_{FS} &= T_{FS}^1 \sqrt{\varepsilon} + O(|\varepsilon|) \end{aligned}$$

We use $\varepsilon = i \frac{\rho_f \kappa \omega}{\eta}$ as the small dimensionless parameter in our asymptotic analysis. Here ρ_f is the density of reservoir fluid, κ is reservoir rock permeability, η is fluid viscosity, ω is the angular frequency of the signal and i is the imaginary unity.

$$R_{FF}^0 = \frac{Z_1^F - Z_2^F}{Z_1^F + Z_2^F}$$

and

$$T_{FF}^0 = \frac{2Z_1^F}{Z_1^F + Z_2^F}$$

Z_1^F and Z_2^F are the impedances of the P-wave above and below the boundary. It is interesting to notice that T_{FF}^1 and R_{FF}^1 depend on the ratio characterizing the contrast between the rock compressibility and fluid mobility in different parts of the reservoir. Approximately

$$R_{FF}^1 \approx T_{FF}^1 \approx 1/(1 + Z_2^F/Z_1^F)$$

If the contrast between the impedances is small

$$R_{FF}^1 \approx T_{FF}^1 \approx 1/2$$

The results above suggest that the amplitude of the slow wave generated by an incident fast wave is small of the order of $\sqrt{\varepsilon}$ relative to the fast wave. The slow wave attenuates exponentially, so its contribution to the reflected signal is small. However, if the layer under consideration is thin, the slow wave can reach the other boundary and generate two pairs of slow and fast reflected and transmitted waves. Asymptotic analysis of the respective reflection and transmission coefficients suggests that the slow-wave-to-slow-wave transmission and reflection coefficients include nonzero frequency-independent terms, whereas the generated fast wave is of a higher-order small component. Due to the exponential decay, the reflected slow wave dies out soon. The generated fast waves from slow wave can be neglected due to the higher order of smallness. Thus, we conclude that in the analysis of the reflection from a layered fractured medium, the role of the slow wave component almost exclusively is limited to affecting the fast wave transmission and reflection through the dissipation of energy in viscous friction.

Finally, the reflection and transmission coefficients are

$$R_{FF} = \frac{Z_1^F - Z_2^F}{Z_1^F + Z_2^F} - \frac{1+i}{2\sqrt{2}} \sqrt{|\varepsilon|} + \dots$$

$$T_{FF} = 1 + \frac{Z_1^F - Z_2^F}{Z_1^F + Z_2^F} - \frac{1+i}{2\sqrt{2}} \sqrt{|\varepsilon|} + \dots$$

The frequency-dependent terms in the last two equations reflects the fact that part of the energy carried by the propagating wave is transferred to the slow wave. The latter quickly dissipates in viscous flow.

Reflection from a reservoir

For reservoir with layered structures, the reflection and transmission coefficients require superposition of the formulas. The functional structure of the result has a similar asymptotic form. In particular, for the reservoir model (Fig.1) we need to calculate the reflection coefficient from the reservoir top, reflection coefficients from the permeable lenses, and reflection coefficient from the reservoir bottom taking into account the transmission coefficients from the lenses.

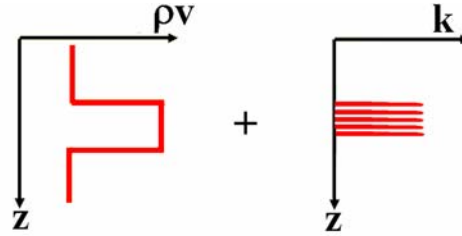


Fig.1. Two media reservoir model with a porous layer (left image) that includes high permeable lenses (right image).

Asymptotically the transmission coefficients from the permeable lenses can be described based on the formulas above. For symmetrical variation of the permeability (Fig.1) and considering different sign of the frequency-independent (first) term of the reflection coefficients from the top and the bottom of the lens, we can write the transmission coefficients for number (N) of high permeable lenses in a simple form:

$$T_L = \prod_N \left(1 + \frac{Z_{n1}^F - Z_{n2}^F}{Z_{n1}^F + Z_{n2}^F} - \frac{1+i}{2\sqrt{2}} \sqrt{|\epsilon_n|} \right) \approx e^{-N \frac{1+i}{\sqrt{2}} \sqrt{|\epsilon|}}$$

In this case the reflection coefficient from the inhomogeneous reservoir with high permeable lenses can be written in the form

$$\begin{aligned} R \approx & R_{FF}^0 - [1 - (R_{FF}^0)^2] \sqrt{i\epsilon} [e^{-i\omega[\Delta t/(N+1)]} + \\ & + \sum_{n=1}^{N-1} e^{-i\omega(n+1)[\Delta t/(N+1)] - 2n\sqrt{i\epsilon}} - \\ & - R_{FF}^0 [1 - (R_{FF}^0)^2] e^{-i\omega\Delta t - 2N\sqrt{i\epsilon}} \end{aligned}$$

Where $\Delta t/2$ is time thickness of the reservoir and $\omega=2\pi f$ is angular frequency.

Based on the description of the reservoir reflection coefficient and reservoir parameters (Table 1 and Table 2) we have calculated the reservoir response with different number of high permeable lenses and different fluid saturation. The reservoir is 20 m thick and water saturation of 100% and gas saturation of 30% are considered.

Table 1 Reservoir rock properties

	Velocity (m/s)	Density (g/cm ³)	Thickness (m)
Surround shale	2643	2.29	
Water reservoir	3048	2.23	20
Gas reservoir	2789	2.08	20

Table 2 Fluid and transport properties

	Density (g/ cm ³)	Viscosity (g/cm s)	Permeability (cm ²)
Water	1.0	0.01	10 ⁻⁸
Gas	0.1	0.00015	10 ⁻⁸

Results of calculations

Two figures below show the behavior of the reservoir reflectivity vs. frequency f for a number of high permeable lenses for both water saturation (Fig.2) and gas saturation (Fig.3). We can see the remarkable influence of the high permeable lenses on the reservoir reflectivity, in particular in case of the gas saturation. There is perceptible shift of the resonance frequencies to low frequency domain if the number of high permeable lenses is increased.

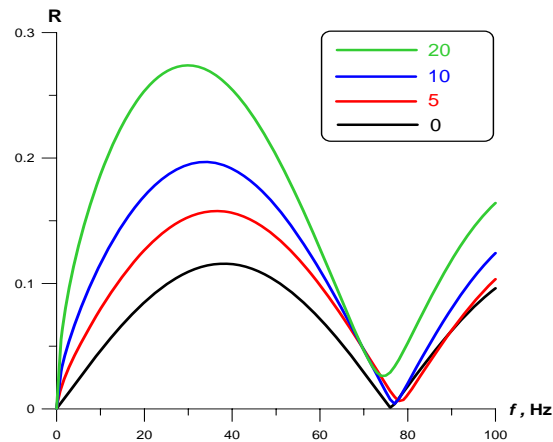


Fig.2. Reflection coefficient from a water-saturated reservoir with different number (0, 5, 10, 20) of permeable lenses.

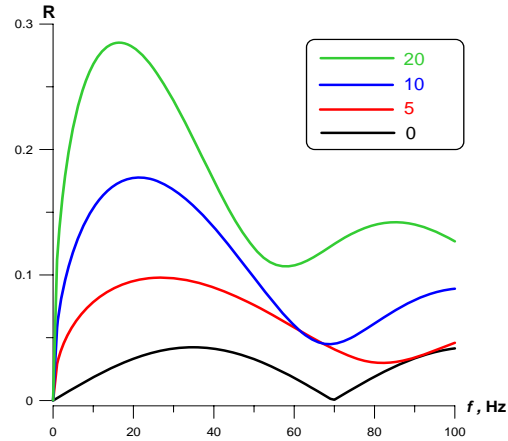


Fig.3. Reflection coefficient from a gas-saturated reservoir with different number (0, 5, 10, 20) of permeable lenses.

We observe a very different reservoir response with fluid substitution for homogeneous porous reservoir (Fig.4) and for inhomogeneous porous reservoir with high permeable lenses (Fig.5).

As expected for a Class 2 homogeneous reservoir model, the gas fluid substitution decreases the peak amplitude dramatically because the impedance contrast is changed. And there is a small shift of the resonance frequency since the gas interval has a larger two-way time. The amplitude spectrum has a symmetrical form (Fig.4).

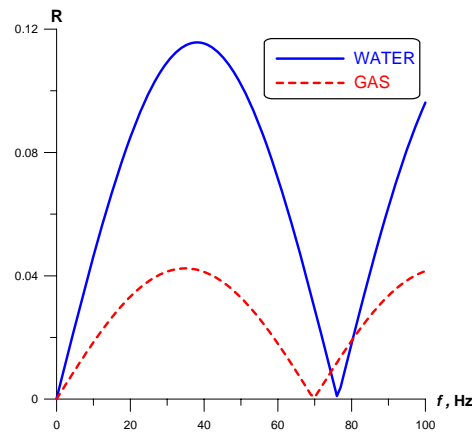


Fig.4. Reflection coefficient from a homogeneous porous reservoir with different fluid saturation

For the inhomogeneous reservoir the gas fluid substitution decreases resonance frequency practically by one half (Fig.4) relatively to water saturation case. And the peak amplitudes for water saturation and gas saturation are comparable. There is no symmetrical form. The amplitude of the reflection from the gas-saturated reservoir is higher at low frequencies and smaller at high frequencies. This is in agreement with numerous field experiments (Goloshubin, et al., 2006).

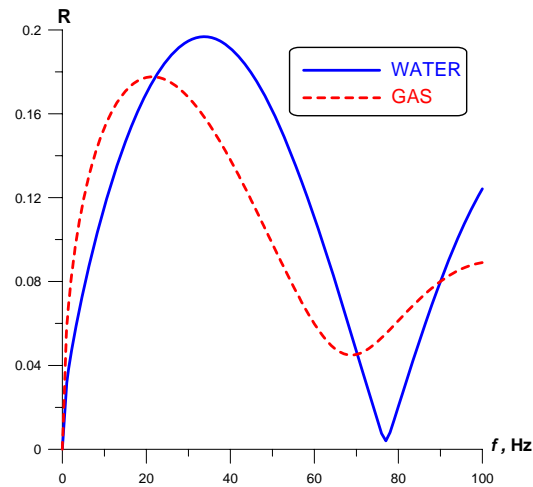


Fig.5. Reflection coefficient from a inhomogeneous porous reservoir with different fluid saturation.

1.2 Amplitude versus offset & frequency

Rutherford and Williams (1980) identified three curves based on amplitude versus offset for gas-saturated reflections. They are AVO Class 1, 2, and 3 anomalies. In this study, we focus on AVO Class 2 anomalies where the seismic amplitudes from gas reservoirs increase with offset. For the equivalent water-saturated reservoir, the amplitude normally decreases with offset.

The AVO Class 2 reservoir model shown in Table 1 is used to illustrate the amplitude spectra of a thin bed saturated with different pore fluids at different incident angles and frequencies. The reservoir is 20-m thick and water saturations of 100% and 30% (gas) are considered. The amplitude spectra for 0° and 30° incident angles and different frequencies are calculated for the water-saturated and gas-saturated case (Figure 6). As expected the peak frequency decreases if the thin-bed time interval increases. Thus, the peak frequency for gas saturation is less than the water saturation since the gas interval has a larger two-way travel time.

It is illustrated in Figure 6 that not only do the spectra amplitude change with frequency, but also the spectra amplitude change with offset. It suggests that frequency-dependent AVO (AVOF) attributes should be useful hydrocarbon indicators.

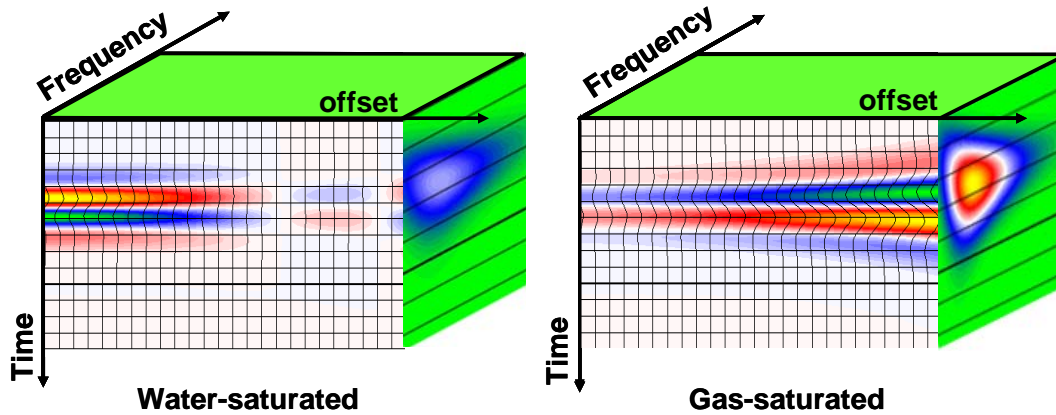


Fig.6. Modeling data: The AVO&F responses from water-saturated reservoir (left) and gas-saturated reservoir (right)

Methodology linkage

To benefit from AVOF observations, we integrate AVO analysis and spectral-decomposition to get a better discrimination between gas- and water-saturated reservoirs. Following Mallat (1999), the short window discrete Fourier transform (SWDT) equation, which is the easiest way to understand spectra-decomposition technique, can be written as

$$U(\tau, f) = \frac{1}{\sqrt{2\pi}} \int u(t)W(t - \tau)e^{-i2\pi ft} dt$$

where, $u(t)$ is seismic data in time domain, τ is the center time of the window function $W(t - \tau)$, f is frequency, and $U(\tau, f)$ is the time-frequency function. For a time window, at any center time τ and frequency f_i , the SWDT can be seen as an average operator. At time τ and frequency f_i , the output, $U(\tau, f_i)$, is the weighted average in the selected window. The weights are the result of the window function $W(t - \tau)$ and $e^{-i2\pi ft}$.

Since, the spectral decomposition technique yields the amplitude at different frequencies, if we cross plot the near-offset spectral amplitudes versus far-offset spectral amplitudes around the optimal frequency, we can benefit from both frequency decomposition and AVO techniques as we observed from the forgoing analysis.

Synthetic example

Figure 7 contains a 2-D reservoir model. A dipping reservoir (marked as 3 and 4) is encased in shale and truncated updip by an unconformity.

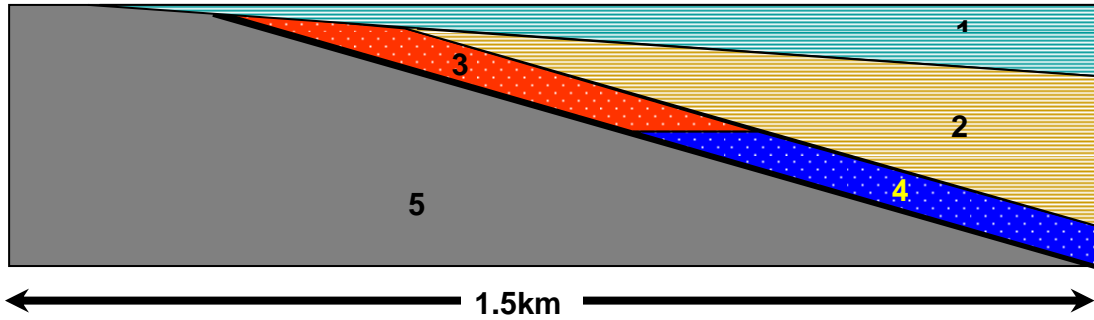


Fig.7. Thin-bed dipping reservoir model (reservoir properties are given in Table 3)

The vertical thickness of the reservoir is 15 m. The upper part of the reservoir is gas saturated and the lower, water saturated. The rock properties (densities and velocities) of each layer are listed in Table 3.

Table 3. Rock properties of synthetic model

Layer names	Vp (m/s)	Vs (m/s)	Density (gm/cc)
1	2530	1081	2.27
2	2643	1168	2.29
3	2789	1650	2.08
4	3049	1595	2.23
5	2695	1208	2.30

Using a 25-Hz Ricker wavelet, the seismic responses are computed for incident angles of 0° and 25°. Using spectral-decomposition, each section is decomposed into different frequency Gabor-wavelets. After spectral-decomposition, the optimal 30-Hz spectral amplitudes for the 0° and 25° incident angles are chosen to cross plot. The cross plot is shown in Fig.8.

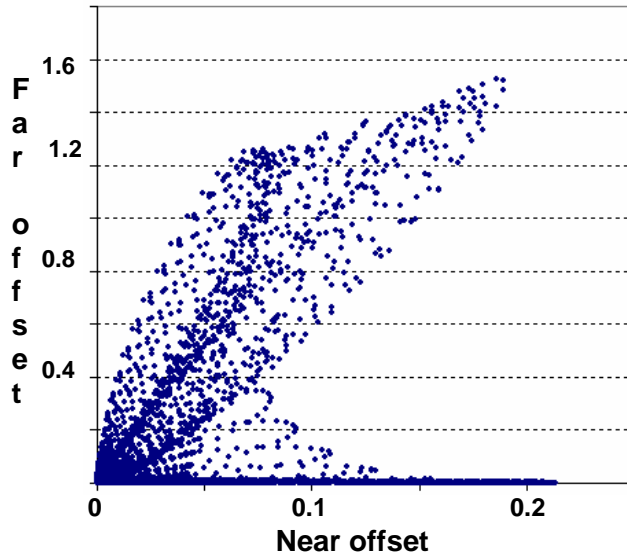


Fig.8. Modeling data: Spectral amplitudes cross-plot

The data points are selected with high slope and high far amplitude values in the cross plot and then mapped back to the seismic section resulting in the section shown on the right of Figure 9. The gas reservoir is clearly illuminated as expected.

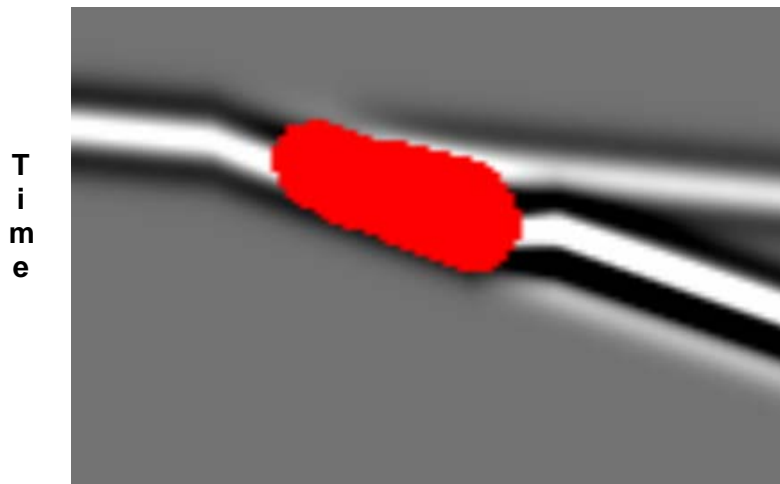


Fig.9. Illuminated gas reservoir on the seismic section

Concluding remarks

We have developed the asymptotic formula based on Biot-Barenblatt model to describe the planar P-wave reflection coefficients from the inhomogeneous porous reservoir with

different types of saturation and a number of high permeable lenses. The numerical study of the reflectivity caused by interlayer fluid flow and scattering in the case of a finely layered permeable reservoir was performed.

The results of the numerical study show remarkable difference between the reflectivity of homogeneous porous layer and porous layer with variation of permeability. It demonstrates a possibility for the investigation of the reservoir transport properties. For the inhomogeneous reservoir, the gas fluid substitution decreases resonance frequency practically by a factor of two relatively to water saturation case. The amplitude of reflection from gas-saturated reservoir is higher at low frequencies. It is in agreement with numerous field experiments (Goloshubin, et al., 2006).

The Spectra Cross plot technique has been developed. This technique integrates AVO and frequency-dependent analyses. Based on the modeling data we found that the Spectra Cross plot technique can be a useful tool for discrimination between gas and wet reservoirs in AVO 2 environments.

2. PHYSICAL MODELING

Milestones:

The proposed milestones of physical modeling are:

- Construct and utilize 3D anisotropic fractured physical model for investigation of wave attenuation within fractured material and azimuth- and frequency-dependent reflectivity of the porous model surfaces.
- Acquire seismic data with wide frequency band (10-300 kHz) for different azimuths and offsets over the model filled with air, water, and glycerin.
- Analyze the attenuation and the frequency-dependent reflectivity for different angles and azimuths of reflections.
- Verify the numerical modeling and the seismic imaging algorithms by comparison with the physical modeling data.

Approach and Accomplishments:

We have successfully acquired, processed and interpreted multi-azimuth 3D surveys across an HTI model made from Plexiglas sheets. The results from the HTI physical model were very beneficial in understanding numerous propagation effects caused by fractures, in particular at far offsets. The significance of these effects for recognizing fracture density and orientation has been discussed at our annual CAGE meeting in December 2005 (Doruelo and Hilterman, 2005). The recent results were presented at 2006 SEG Meeting in New Orleans (Doruelo, Hilterman, and Goloshubin).

2.1. Experiment Set-Up and Data Acquisition

We performed our seismic modeling experiments at the University of Houston Allied Geophysical Laboratories physical modeling facility. With the exception of the actual physical models, all variables were kept constant during the experiments. We used the

same ultrasonic spherical transducers throughout the study. The (relative) positions of the transducers above the physical models as well as the survey geometry were kept identical for all experiments. Our source transducer emits a pulse signal with central frequency of about 300 kHz, which scales to a seismic wavelet with central frequency of 30-Hz in field data (scale factor is 1 to 10,000). Given the P-wave velocities of our physical models, the source wavelet will have dominant wavelengths in the order of 8-10 mm or roughly 80 - 100 m in the real world. The entire physical modeling setup (e.g. transducers, fracture and solid Plexiglas models) was completely underwater during the experiments so the resulting seismic records are comparable to conventional marine streamer data. Fig.10 illustrates the physical models and Table 4 provides the properties of the models.

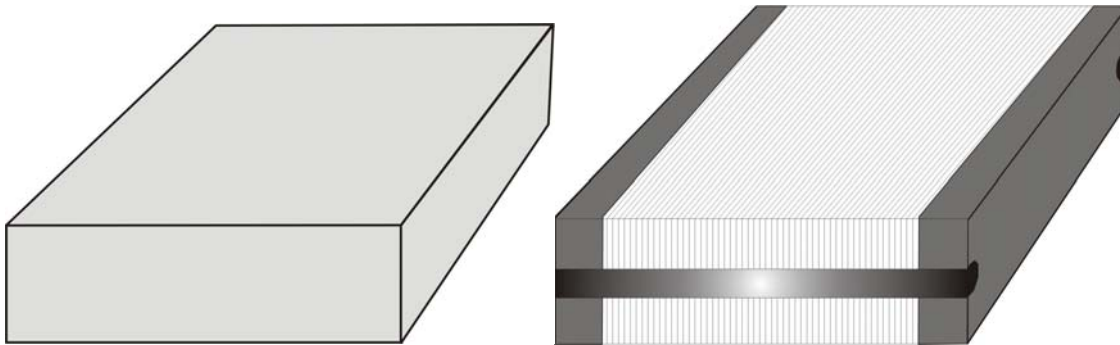


Fig.10. Physical Models: solid Plexiglas (left) and fracture Plexiglas model (right)

Table 4. Properties of the Physical Models

SOLID PLEXIGLAS MODEL		FRACTURE PLEXIGLAS MODEL						
P-wave Velocity	S-wave Velocity	Component Properties			Effective Bulk Properties			
2764 m/s	1385 m/s	Plexiglas sheets (120 pcs)	Parameter	Actual	Scaled (10 000)	Effective HTI Medium	Measured Velocity using Contact Transducers	
			thickness	$\sim 1.4 \times 10^{-3}$ m	14 m		qP-wave velocity ($V_{p \text{ par}}$) parallel to fractures ~ 2684 m/s	$\delta \sim -0.023$
			space* between Plexiglas sheets	$\sim 5.5 \times 10^{-5}$ m	0.5 m		qP-wave velocity ($V_{p \text{ perp}}$) $30^\circ, 60^\circ$ to fractures $\sim 2610, 2641$ m/s	
			P-wave velocity (V_p)	~ 2150 m/s	*filled with water		qP-wave velocity ($V_{p \text{ perp}}$) perpendicular to fractures ~ 2584 m/s	
		Steel Plates	thickness $\sim 1.4 \times 10^{-3}$ m		torque applied (on bolts) ~ 13.56 Nm (10 ft-lb)	V_p anisotropy $\sim 3.7\%$	$\gamma \sim -0.023$	
				(slow) S-wave velocity ($V_{s \text{ par}}$) parallel to fractures ~ 1370 m/s		(slow) S-wave velocity ($V_{s \text{ perp}}$) perpendicular to fractures ~ 1180 m/s		$\varepsilon \sim -0.038$

We shot common-midpoint (CMP) surveys over a solid Plexiglas block and the Plexiglas fracture model and implemented a uniform seismic processing sequence to the collected CMP data. Our processing workflow consisted of gain corrections for spherical divergence and application of filter operators designed primarily for removing the direct arrivals especially in the far-offset traces where they interfere with both head waves and supercritical reflections. Fig.11 shows a CMP gather before and after we ran the standard seismic processing workflow.

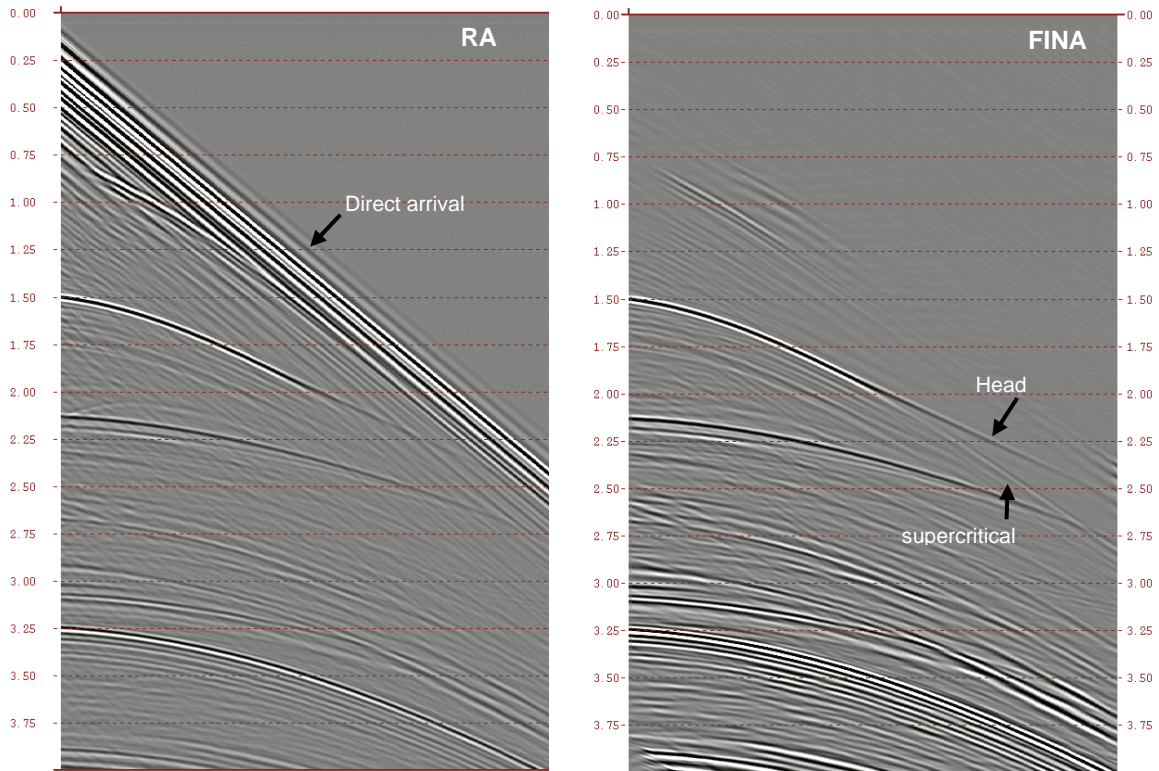


Fig.11. CMP gather before (left) and after (right) processing

The CMP inline collected over the isotropic Plexiglas block was used to calibrate the physical modeling setup. We compared the processed CMP data collected over the solid Plexiglas model and the corresponding seismogram from a reflectivity model with the same parameters as the water-solid Plexiglas experiment and computed their respective AVO responses (Fig.12). Empirical P-wave reflectivity slightly differs from the theoretical values with errors of about $\pm 10\%$. Still, the excellent match between the two curves bears out the accuracy of our physical modeling system in reproducing the AVO signature of isotropic media (Fig.13).

We subsequently collected identical CMP surveys over the fracture Plexiglas model at different azimuth angles relative to the fractures with the same modeling setup as in case of solid Plexiglas model. For the fracture experiments, the midpoint of all CMP inlines lies at the geometric center of the fracture model and a given inline is set at an azimuth angle measured with respect to the strike direction of the fractures. We shot CMP surveys at equal azimuth intervals of 15° for inlines ranging from 0° to 345° azimuths, collecting a total of 23 CMP gathers. The 10 000 - scaling factor applied in both space and time allowed us to directly compare our physical modeling data with the numerically-derived synthetic seismograms. Actual experiment parameters are listed in Table 4 along with their scaled values in a corresponding field survey.

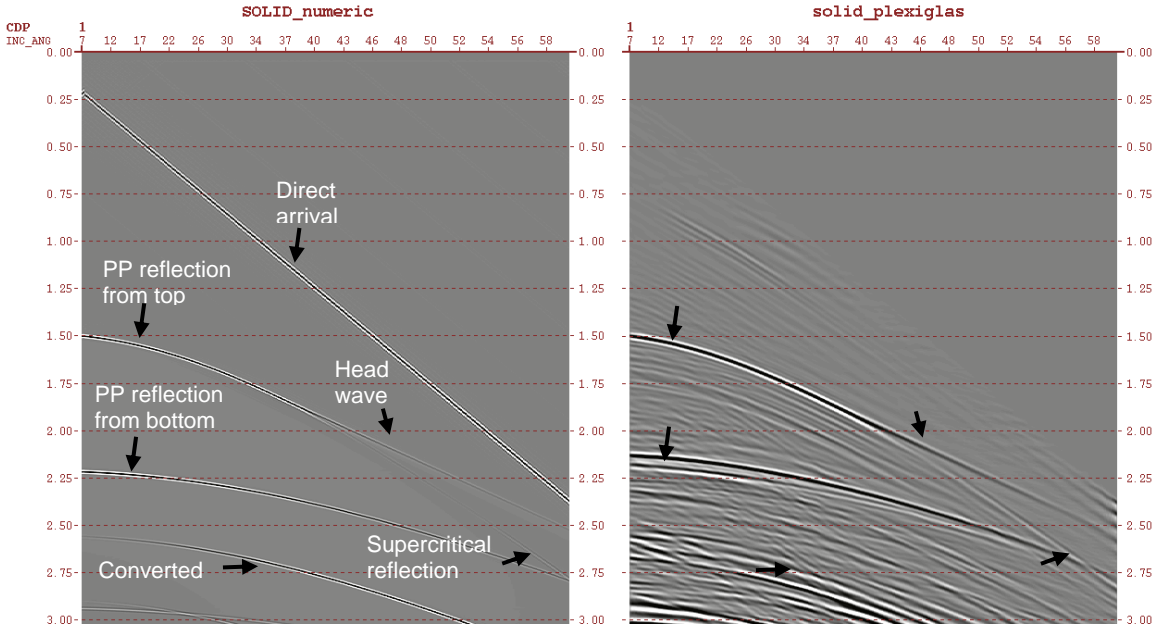


Fig.12. Numerical CMP (left) vs. Experimental CMP (right)

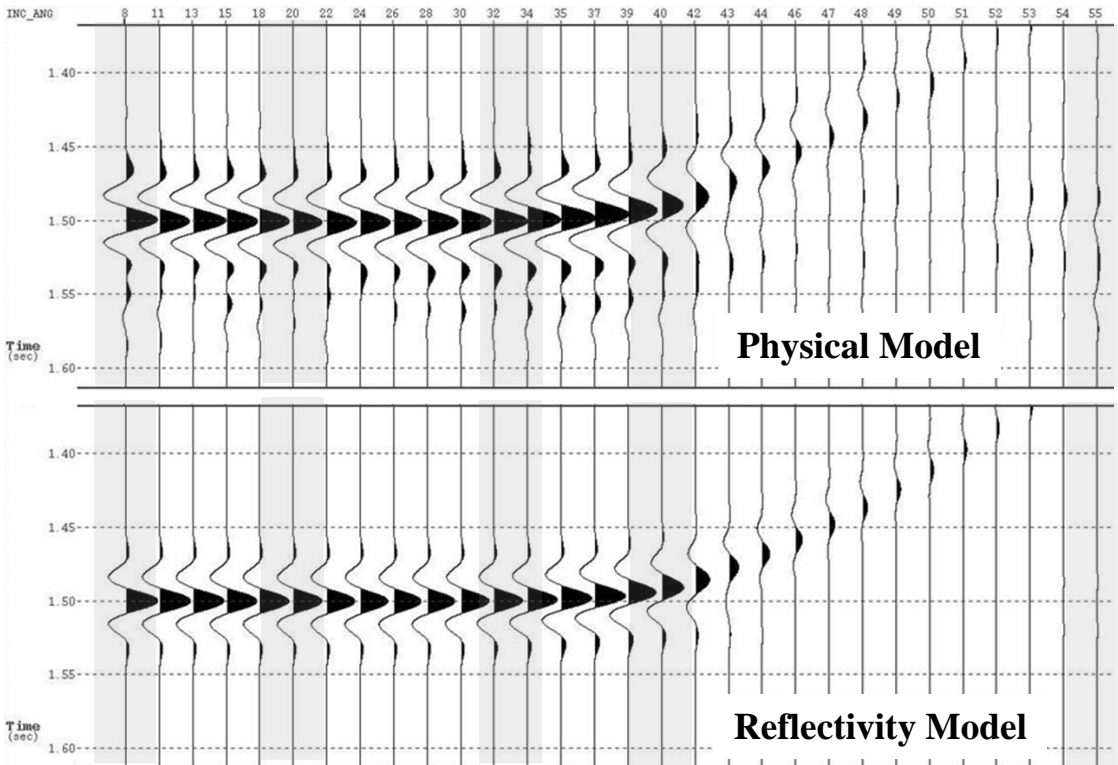


Fig.13. PP reflection from the surface of the solid model after linear move out correction. Numerical CMP (bottom) vs. Experimental (upper part)

Direct V_p measurements reveal that statically our physical fracture model can be treated as an HTI effective medium. We also measured head wave velocities in the azimuthal CMP gathers to assess if the effective medium assumption is valid from a kinematic standpoint. Pure head waves are generated when spherical (seismic) waves in a lower-velocity medium are incident upon a medium of higher velocity. At the critical angle, head waves appear and propagate with the same P-wave velocity as that of the fractured medium. Head waves will occur in our physical fracture experiments because the lowest possible effective V_p (2584 m/s) of the fracture model is still higher than the water velocity (1500 m/s). Moreover, the head waves are expected to have different velocities depending on the azimuth of the CMP gathers. Where head waves can be precisely identified in the CMP records their velocity will correspond to the effective V_p of our fracture model at that azimuth direction where the CMP inline was collected. Static correction of the CMP gathers using linear moveout velocities lines up reflections so that head waves appear as flat coherent events after the critical region. The linear moveout velocity corresponds to the velocity of the head waves and by extension the velocity of the refracting medium. Figure 14 (left) shows CMP inlines collected over the fracture model at 4 different azimuths relative to the strike of the fractures.

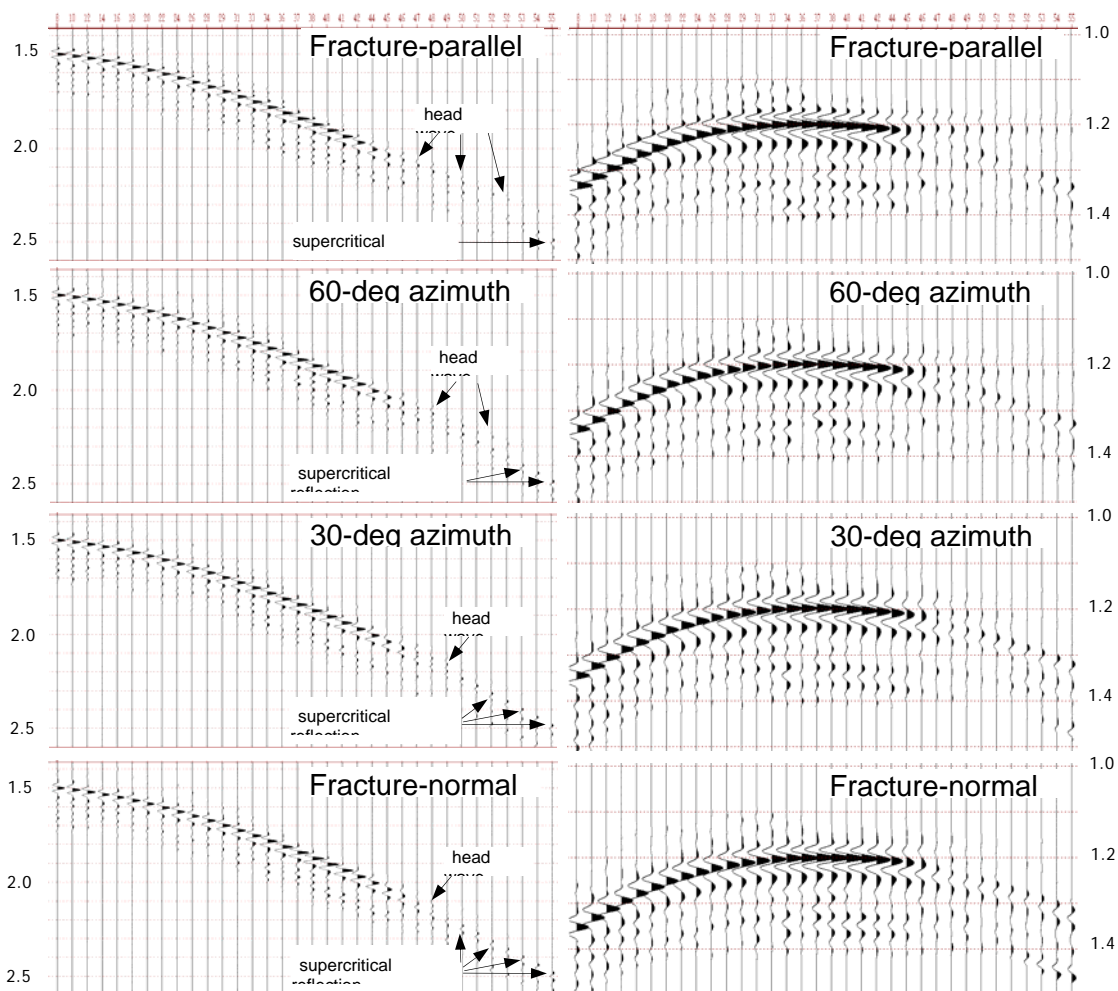


Fig.14. Fracture Model CMP gathers at different azimuths (left) and the same after linear moveout correction (right)

We uniformly applied a matched filter to all our CMP gathers making our impulse wavelet nearly zero-phase and so the arrival of reflections is marked by the highest peak amplitude in the pre-critical region. We then applied static corrections to each CMP inline using different linear moveout velocities (Figure 14, right). Compared to the source wavelet, far-offset refraction events are normally of lower frequency and are -90° phase-shifted (Cerveny and Ravindra, 1971). Consequently, the correct linear moveout velocity for flattening the head waves will line up the peak amplitude of the reflections just before the critical angle to the zero-crossings of the -90° phase-shifted refraction wavelet. The most suitable moveout velocity is equivalent to the head velocity and it is approximately equal to the effective velocity of the fracture model at the particular azimuth where the CMP inline was recorded. Plotting the different moveout velocities as a function of inline azimuth yields the azimuthally-varying P-wave velocity of the effective HTI medium. Figure 15 shows the head wave velocities as a function of CMP inline azimuth.

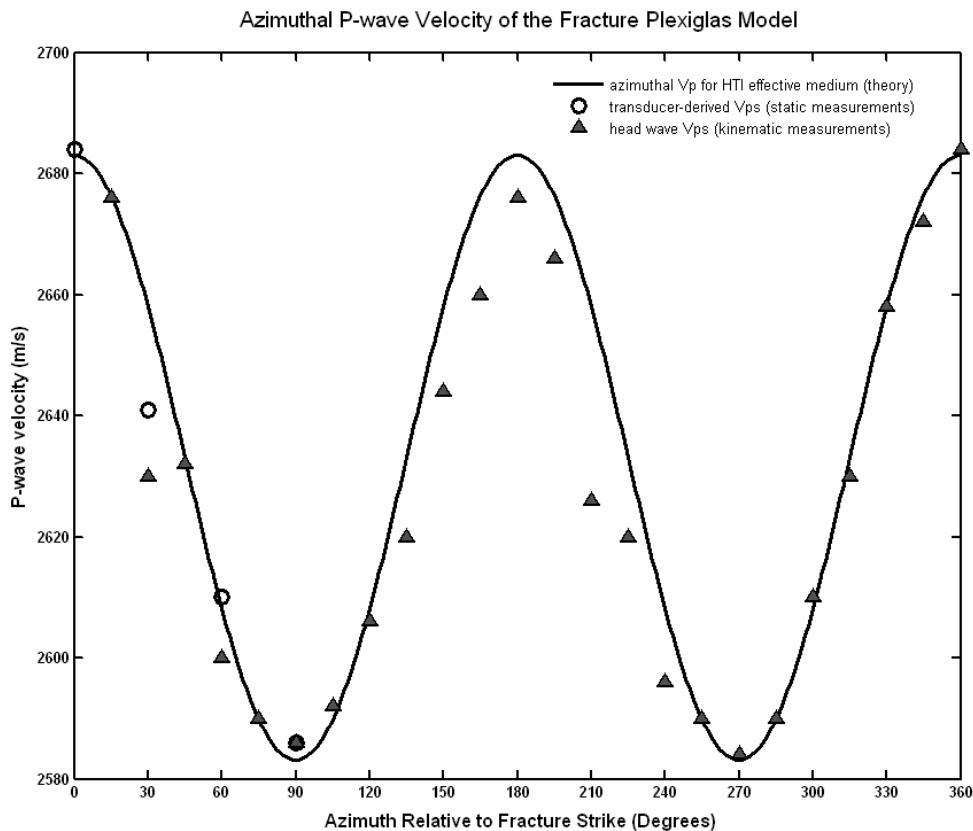


Fig.15. P-wave velocity vs. azimuth. In kinematic sense the fracture Plexiglas model equivalent to HTI medium.

Included in the same figure are P-wave velocity measurements using contact transducers and the theoretical curve for the azimuthally-varying P-wave velocity of an effective HTI medium equivalent to our Plexiglas fracture model. The excellent fit of the measured V_p as a function of azimuth to the theoretical V_p vs. azimuth curve confirmed that in both static and kinematic sense our Plexiglas fracture model behaves as an effective medium

with HTI symmetry. Amplitude Variation with Offset and Azimuth (AVOA) is not so clear.

2.2. Amplitude vs. Azimuth

Reflection amplitudes from a vertically-fractured (HTI) medium depends on two angles – the polar incident angle between the vertical and the slowness vector of the incident wave and an azimuthal phase angle that is defined with respect to the HTI symmetry plane (Ruger and Tsvankin, 1997). Ruger’s equation of P-wave reflectivity at the horizontal boundary between an isotropic medium and an anisotropic medium with HTI symmetry provides a good approximation of azimuth-dependent AVO response of fracture media at small incident angles. We therefore compared the pre-critical angle ($< 34^\circ$) AVOA of our fracture Plexiglas model with the analytic AVO of a corresponding HTI medium computed at various azimuths using Ruger’s (1997) AVO equation (Fig.16).

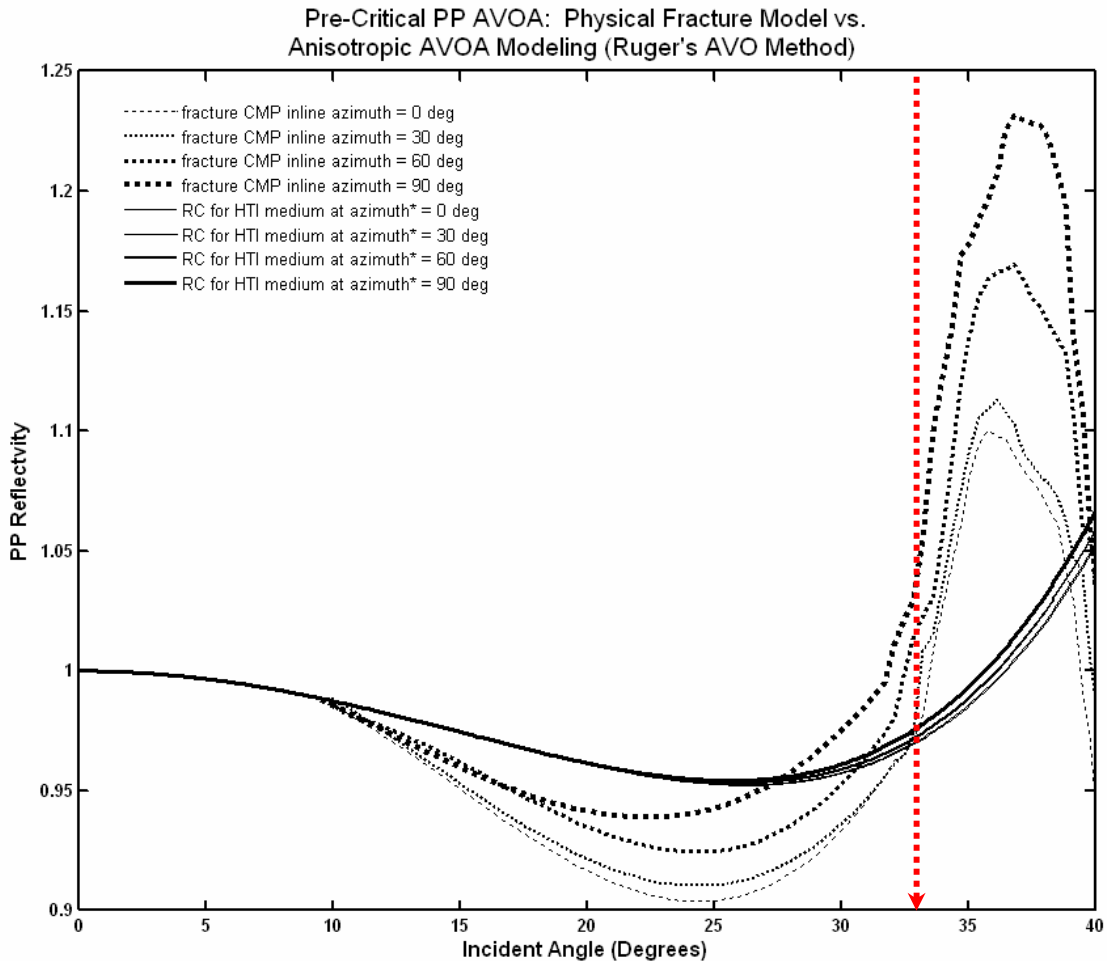


Fig.16. Amplitude vs. azimuth: numerical data (solid line) and experiments (dotted lines)

In our experiments, we collected the CMP inlines relative to the fracture strike direction and so the azimuths of our survey (and data) are referenced to the isotropy axis of the effective HTI model. We adapted Ruger’s convention for our inline azimuth notation

though for our CMP fracture gathers, we will still refer to azimuthal phase angles 90° and 0° as fracture-parallel and fracture-perpendicular CMP inlines respectively.

The AVOA response of our fracture Plexiglas model deviates from the analytic AVOA of an equivalent effective HTI medium only at higher incident angles but the maximum difference (<7%) between the two sets of AVOA curves is small and well within the precision capability of our physical modeling facility. Therefore, the overall match between the AVO curves of the physical fracture model and the corresponding numeric HTI medium in the pre-critical region is good. Especially obvious is the similarity in the AVO gradients as a function of azimuth. For very thin but water-wet cracks the AVO gradient in the HTI isotropy plane or in the fracture-parallel CMP data becomes more negative with increasing incident angle and more so compared to other azimuth directions. Ruger's equation predicts this result since the difference in symmetry plane (AVO) gradients for wet fractures (*i.e.* approximately $\delta^{(v)} + 2\gamma$) becomes more negative with increasing azimuth phase angle. In our physical modeling experiments, this happens when the CMP inlines becomes increasingly parallel to the fracture strike directions. The pre-critical AVOA response of our fracture model thus obeys Ruger's anisotropic AVO formula.

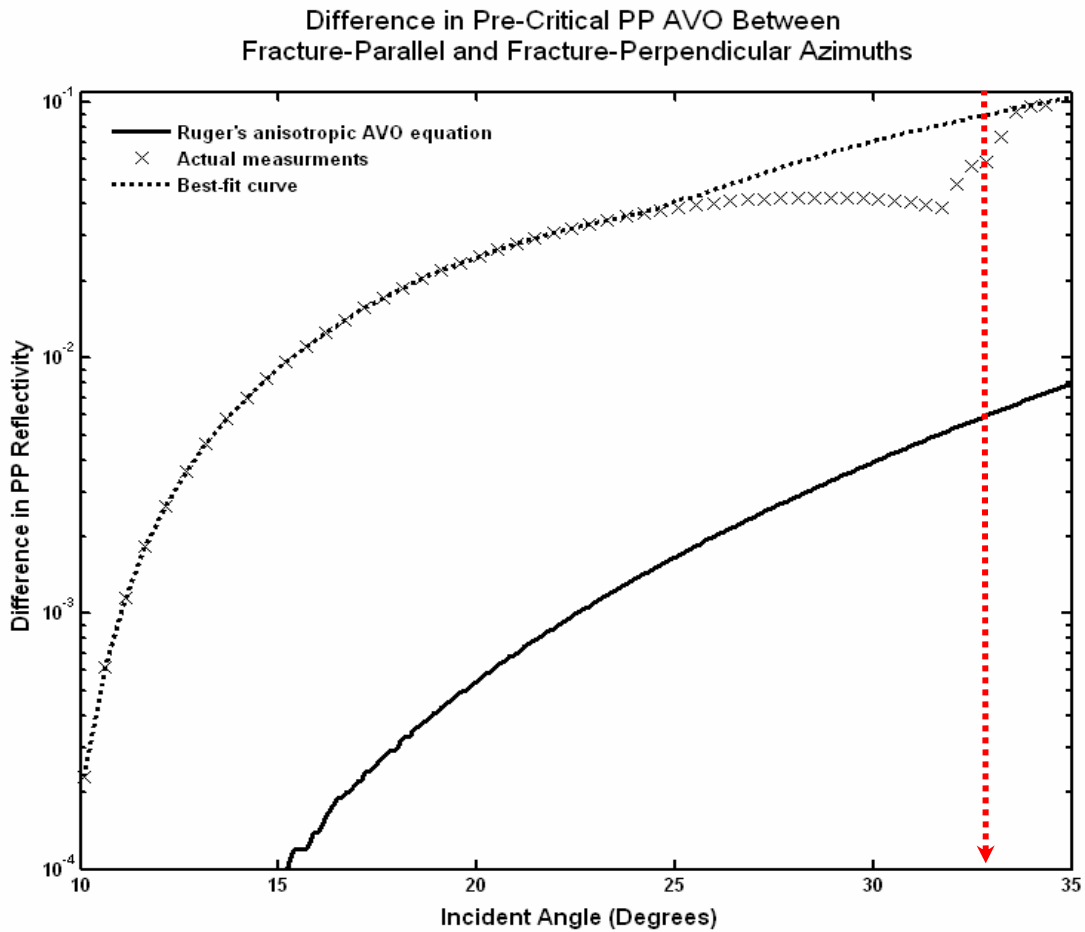


Fig.17. Residual AVOA

The pre-critical region AVOA plots also revealed another important result. Subtracting any two AVOA curves from the same model (fracture or HTI) yields an AVO residual curve that has higher magnitudes for the fracture seismic experiments than in their corresponding numeric solutions. Figure 17 shows the magnitude of the difference in AVO response in the symmetry and isotropy planes for the fracture analog and its equivalent HTI medium. A best-fit line drawn through the measured AVO residuals between fracture-parallel and fracture-perpendicular CMP gathers resembles the AVO residual curve for the isotropy and symmetry planes of the anisotropic HTI model yet the fracture AVO residual is up to one order of magnitude greater than the numeric AVO residual even in the pre-critical offsets. Lynn *et al.* (2004) noted that such incongruence between theoretical AVOA and actual AVOA measurements is frequently observed in field data.

The AVOA response of the fracture Plexiglas models progressively deviates from AVOA numeric solutions (Ruger's approximation) just before the critical angle. Significant departure of our empirical results from the predictions of anisotropic AVO theory suggests that fundamental physical processes influence the amplitudes of the critical and post-critical fracture reflections but are still not fully understood. The numeric methods highlighted the discrepancy between standard approximations of anisotropic AVO and actual P-wave reflectivity derived from our physical model seismograms, especially in the regions close to and beyond the critical incident angle (Fig.16). Our experiment shows that head waves influence PP AVO magnitudes depending of the (CMP) inline azimuth to the fracture symmetry plane. Head waves variably interfere with reflections in the critical region and the ultimate effect is for the amplitude of reflection and interference head waves in the critical region to be almost 20% higher for CMP inline azimuth perpendicular to fractures than it is for fracture-parallel CMP inlines. Moreover, the supercritical reflection amplitudes are also sensitive to fracture orientation with CMP inline perpendicular to fractures showing brighter reflection amplitudes compared to supercritical reflection in fracture-parallel CMP data. We propose that head waves contribute a first-order influence on AVOA in the critical regions of reflection field data. In the supercritical region, the decrease in shear modulus in the fracture-perpendicular azimuth accounts for the dramatic difference in amplitudes of reflections in the fracture-parallel vs. fracture-perpendicular azimuths. The head wave effect on AVOA, though never included in standard AVO analysis, is crucial for accurate seismic fracture characterization.

3. THEORY VERIFICATION WITH FIELD DATA

Milestones:

The proposed milestones are:

- Reprocess the existing 3D seismic data with preserved amplitudes and frequencies.
- Estimate frequency-dependent seismic attributes.
- Build the geologic models of reservoir.

- Calibrate the frequency-dependent seismic attribute against the geologic models and reservoir parameters determined from petrophysical and engineering data.
- Map fluid contacts and permeability variation and/or production rate of hydrocarbons.

Approach and Accomplishments:

3-D seismic, geologic, borehole, and engineering data have been acquired for the project study areas. Our four 3-D seismic data come from three offshore areas East Breaks, High Island and South Marsh Island in the Gulf of Mexico, and from the onshore region of the Central Basin Platform, West Texas. We have loaded all 3-D data sets in the interpretation system, Geoframe, and all near, far and full stacks into the seismic processing system, Focus. All the data have been loaded and preliminary interpretations and reprocessing have been done. We have described the initial structural and stratigraphic interpretation of the various seismic volumes.

We have developed rock-property transforms. These transforms were derived from rock-property trends of 500 reservoirs in both the shelf and deep-water Gulf of Mexico. With these two transforms and the AVO gathers at the prospect and at the down-dip water-equivalent reservoir, a test statistic can be developed that estimates the pore-fluid saturation. The methodology doesn't require a calibration well that ties the seismic unless the bed thickness is desired. The results were presented at 2005 SEG Meeting in Houston (Zhou, Hilterman, Ren, and Kumar) and 2006 SEG Meeting in New Orleans (Zhou, Hilterman, and Ren).

We have provided frequency decomposition and frequency-dependent amplitude analysis of the reflected waves from the hydrocarbon-saturated reservoirs based on our theoretical investigations. The results were presented at 2005 SEG Meeting in Houston and 2006 SEG Meeting in New Orleans (Goloshubin and Silin).

The Spectra Cross plot technique has been developed and tested. This technique integrates AVO and frequency-dependent analyses. Based on the analysis of the field data we found that the Spectra Cross plot technique provides a quick and useful tool for discrimination between gas and wet reservoirs in AVO 2 environments. The results will be presented at 2007 SEG Meeting in San Antonio (Ren, Goloshubin, and Hilterman).

3.1. Rock-Property Transforms

The Sw estimation method proposed by Zhou et al. (2005) compares the AVO response from the down-dip wet reservoir to the AVO response from the prospect. To quantify the amplitude differences, two rock-property transforms are employed. One is the pore-fluid transform that relates the reservoir's NI when it is hydrocarbon saturated to the NI when it is wet. The other is the linear lithology transform and this relates the far-angle reflection to NI for different Sw and pore fluids. The concept of this method is to predict the NI-gas and NI-fizz for the both prospect and down-dip locations and then choose the Sw that better matches at both locations. The method includes two assumptions. The

porosities of the prospect and down-dip reservoirs are the same (Assumption 1). Also, the amplitude of the far-angle stack is scaled properly to the near-angle stack during processing (Assumption 2).

A South Marsh Island (SMI) time map shown in Figure 18 contains a gas reservoir. The depth of this reservoir is around 9500 ft.

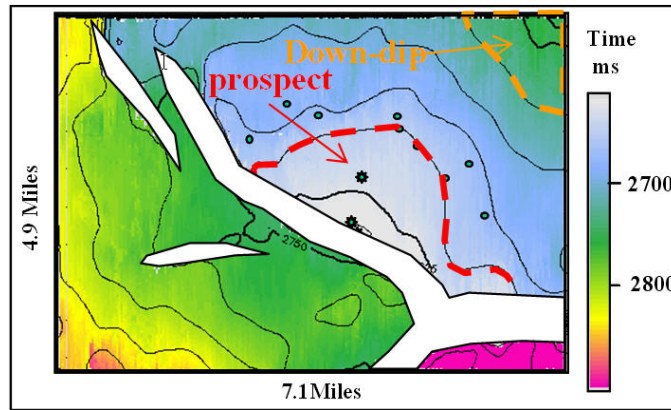


Fig.18. Time map in SMI

Based on the analyses of sand thickness from several wells; we determine that inside the red dash line is the gas reservoir. Down-dip equivalent wet reservoir is inside the yellow dash line. The near-angle and far-angle amplitude maps for this horizon are shown in Figure 19.

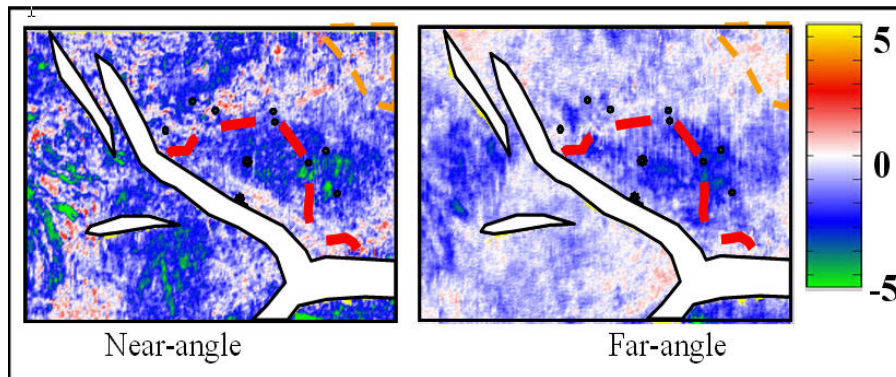


Fig.19. Near- and far-angle amplitude maps of the horizon

For the down-dip part, the wet lithology transform is applied to yield the NI-wet map, shown in Figure 20a.

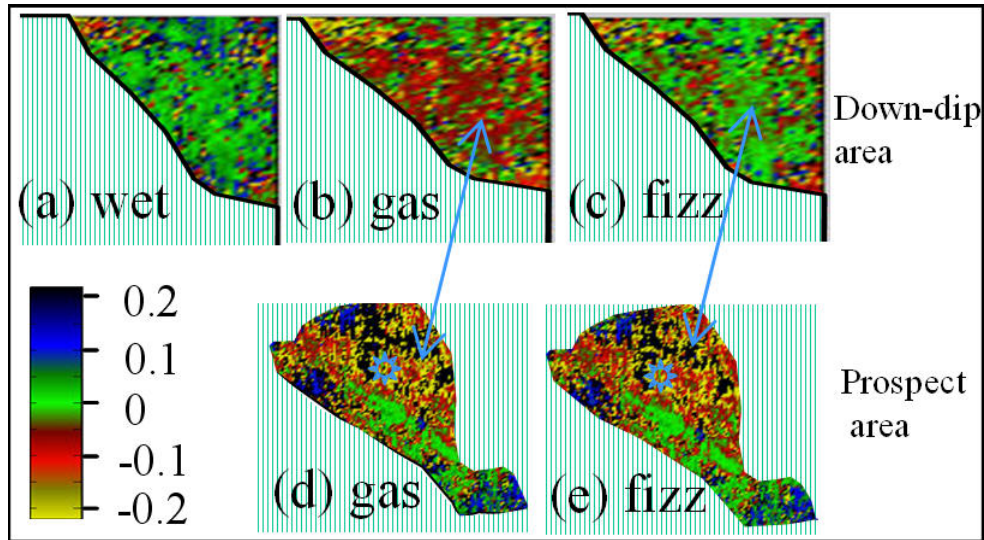


Fig.20. Comparing down-dip NI values for various Sw fluid substitutions to respective lithology transforms at prospect area

Pore-fluid transforms for gas and fizz are applied to the map in Figure 20a to yield the NI-gas and NI-fizz maps respectively, which are shown in Figures 20b and 20c. For the prospect area, both gas and fizz lithology transforms are applied and yield the NI-gas and NI-fizz in the prospect area, which are shown in Figures 20d and 20e.

We need to take into account that in real data, our assumptions are not always satisfied. With a slight change of porosity in the down-dip location, the method is incorrect. We have investigated the sensitivity of the assumptions associated with the new method for predicting pore-fluid type and saturation using seismic amplitudes and rock-property transforms. The results of the investigation were presented by Zhou et al. (2006) at the Annual International SEG Meeting.

3.2. Amplitude vs. Frequency

Our theoretical investigation (see Section 1) indicates that the inhomogeneous high permeable hydrocarbon-saturated reservoirs strongly reflect low-frequency seismic energy and can produce reflection signal, which is noticeable dependent on the frequency and reservoir fluid mobility. This frequency-dependence phenomenon was, in particular, detected in 2D and 3D seismic data from different hydrocarbon fields in different areas (Goloshubin, et al., 2006). Here is an example of frequency-dependent seismic amplitude analysis.

A 3D seismic and well data set was used to investigate frequency-dependent effects from the reservoir zone. The 3D seismic data were recorded using conventional acquisition technology. The frequency-dependent processing and interpretation were carried out to get frequency-dependent images, in particular, in low-frequency domain. There were several important aspects of the processing: a) the relative amplitudes of the seismic data

were preserved throughout the entire procedure; b) the processing retained the broadest possible signal band in the data, preserving the low-frequency domain of the spectrum. Frequency decomposition technique was used for frequency-dependent imaging of the reservoir zone. The Fig.21 (a) illustrates the input 3D seismic data. Frequency-dependent attribute maps along with the reservoir surface are presented in Fig.21 (b) and Fig.21 (c).

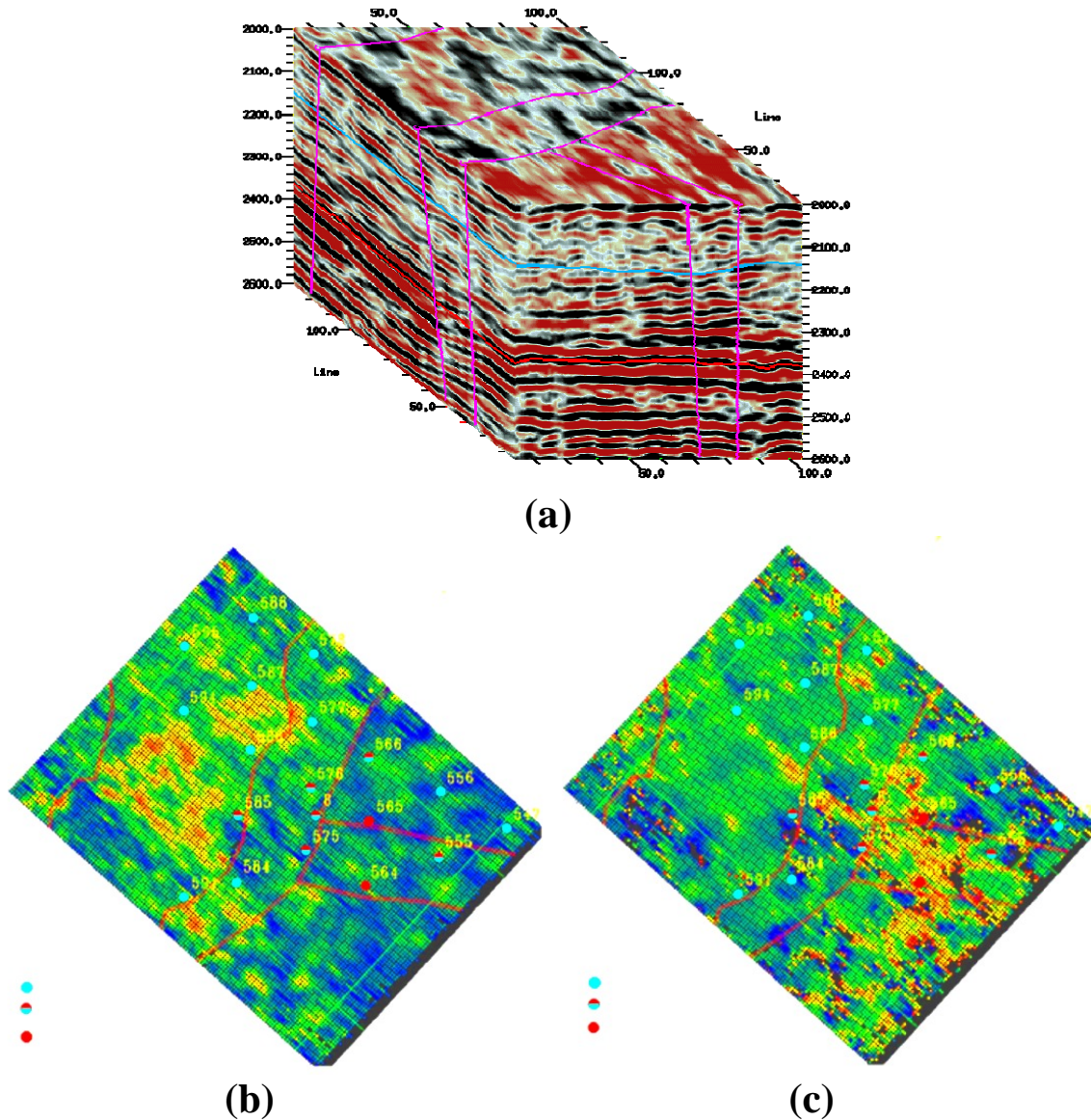


Fig.21. (a) 3D seismic data. (b) map presents the high frequency (50 Hz) amplitude image. (c) map shows the image of the first derivative over frequency at low frequency (10 Hz). Red lines indicate faults and red circles show the positions of the wells with oil and relatively high oil production rate. Blue circles show the positions of the wells with water. Amplitude anomalies at high frequency (b) are connected with clay content within reservoir pore space. Anomalies of low-frequency image (c) indicate oil-saturated reservoir zone with high permeability.

The data from the well logs indicate that the sandstone reservoir is 10-12 m thick, and is 3 km deep. The reservoir porosity varies between 0.16 and 0.18 and the permeability does not exceed 100 milli-Darcy. The produced fluid composition and production rates vary from well to well. Core analysis shows that the clay content within the pore space increases with depth. Clay content has a strong impact on the reservoir transport and mechanical properties. High-porosity and high-permeability material is distributed close to crest of the structure.

Analysis of seismic data suggests that the wells with the highest oil production rate are located close to the fault zones. This observation implies that fractures resulting from faulting may contribute significantly to the permeability of the reservoir. The middle map (Fig.21b) shows variation of the amplitude of the target reflected wave at high frequency (50 Hz). There is a link between the amplitude anomalies and clay content, since the presence of clay modifies the impedance contrast. The wells with the highest oil production rate (red circles) are located near the zones of the high deviation of the map of the first derivative with respect to the frequency obtained at low frequency (10 Hz). It is clear that frequency decomposition and frequency-dependent analysis, in particular at low frequency domain enhances detection of the hydrocarbons and provides information about reservoir fluid mobility properties.

3.3. Amplitude vs. Offset and Frequency

We have used AVAF analysis to illuminate a gas-saturated reservoir zone. A near-offset seismic section is shown on the left of Figure 22, and the equivalent far-offset section on the right.

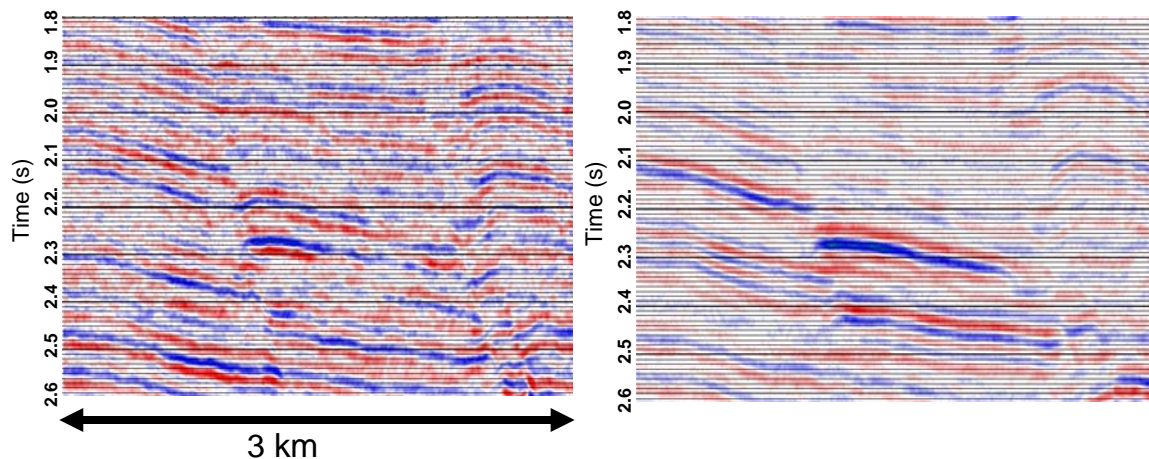


Fig.22. Seismic sections for near offsets (left) and far offsets (right) from 3-D survey in Gulf of Mexico. Data is courtesy of Fairfield Industries.

The 3-D survey is located in the Gulf of Mexico and the line shown has a length of about 3 km. The sediments are clastic sand and shale deposits. It is in an AVO Class 2

environment. Spectral-decomposition was done for the near- and far-offset sections, and the trace number, time and frequency data cube was plotted in Figure 23.

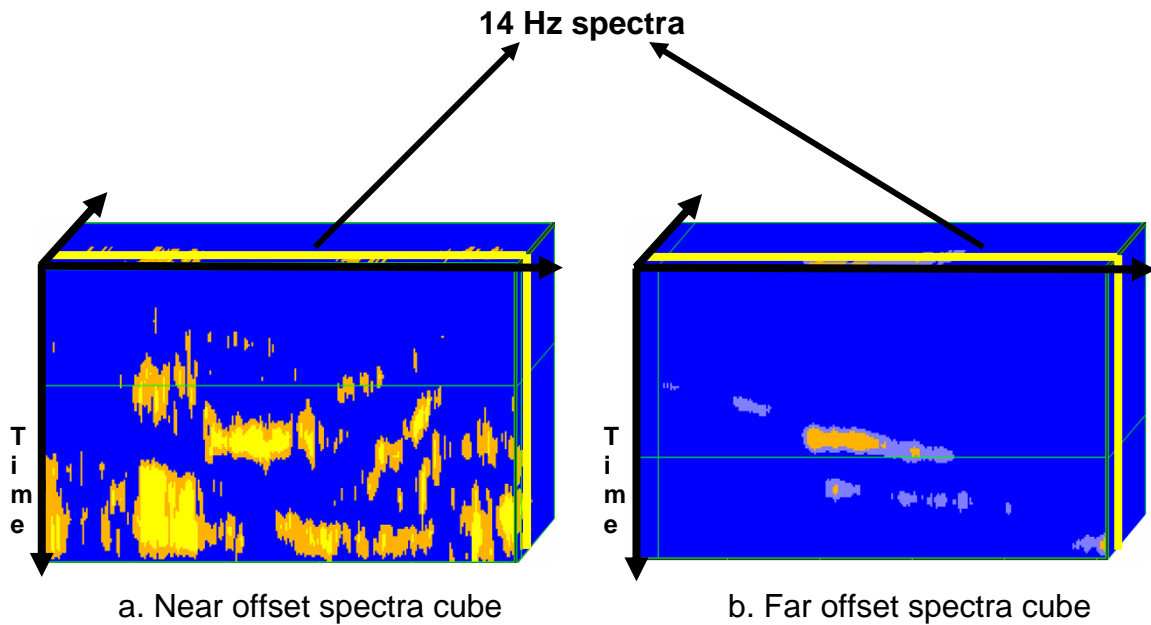


Fig.23. Spectra decomposition cubes for seismic shown in Figure 22

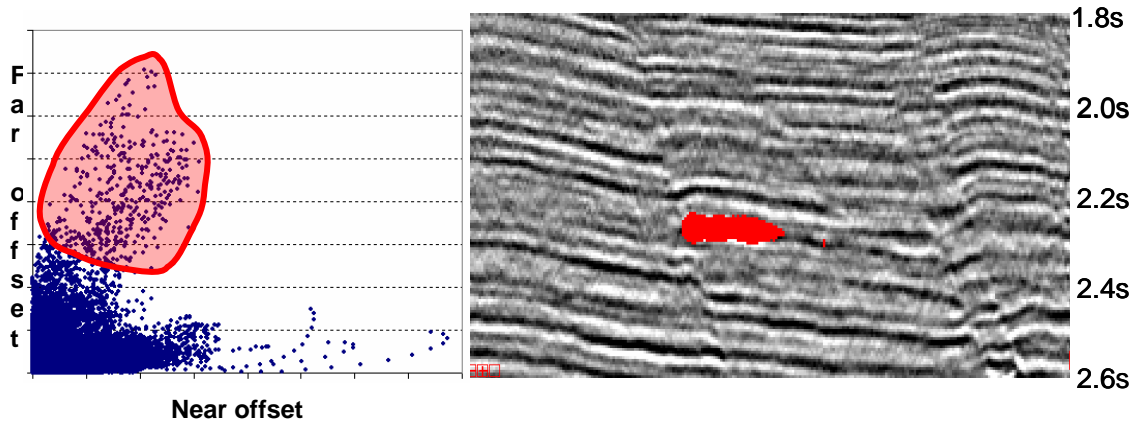


Fig.24. Spectra decomposition trace amplitudes for 14-Hz components taken from vertical sections shown in Figure 23. At left, the spectra cross plot between trace amplitudes from near and far incident angles is shown. Right portion illustrates the red section picked on the cross plot.

The 14-Hz components of near and far spectral amplitudes are cross-plotted. It is shown on the left of Figure 24. If we selected the points with high slope and large values as circled in Figure 10 and mapped them back to seismic data, we get the seismic section shown on the right of Figure 24. The gas reservoir, which was proven in this field, was clearly illuminated by the spectra cross plot.

CONCLUSIONS

Our objective was the development and application of the new techniques that will improve both the delineation and characterization of a hydrocarbon reservoir using variations of seismic amplitude as a function of incident angle and frequency.

We have developed an asymptotic model and governing equations describing low-frequency wave propagation in dual-porosity media. The coefficients of normal reflection and transmission of a planar p-wave from a boundary between two layers in the reservoir were studied in low-frequency range. The coefficients are expressed as power series with respect to small dimensionless parameter, which is product of the frequency and reservoir fluid mobility.

We have successfully acquired, processed and interpreted multi-azimuth 3D surveys across an HTI model made from Plexiglas sheets. The results from our test the HTI physical model were very beneficial in understanding numerous propagation effects caused by fractures.

We have described the initial structural and stratigraphic interpretation of the various seismic volumes. We have formulated and developed rock-property transforms that allow conventional seismic horizon maps to be converted into reflectivity maps. These transforms were derived from rock-property trends of 500 reservoirs in both the shelf and deep-water Gulf of Mexico. With these transforms and the AVO gathers at the prospect and at the down-dip water-equivalent reservoir, a pore fluid saturation can be estimated without a calibration well that ties the seismic unless the bed thickness is desired.

We have developed frequency-dependent amplitude analysis of the reflected waves from the hydrocarbon-saturated reservoirs based on our theoretical investigations. Frequency decomposition and frequency-dependent analysis at low frequency domain enhances detection of the hydrocarbons and provides information about reservoir fluid mobility properties.

The Spectra Cross plot technique has been developed and tested. This technique integrates AVO and frequency-dependent analyses. Based on the analysis of the field data we found that the Spectra Cross plot technique can provide a quick and useful tool for discrimination between gas and wet reservoirs in AVO 2 environments.

As the result of our activity we have published a number of papers and expended abstracts (see **Technology Transfer**).

TECHNOLOGY TRANSFER

The following are our published papers and expanded abstracts:

- Zhou, Z., Hilterman, F., Ren, H., and Kumar, M., 2005, Water-saturation estimation from seismic and rock-property trends, 75th Annual International Meeting, SEG, Expanded Abstracts, 258-261.
- D. Silin, V. Korneev, G. Goloshubin, and T. Patzek, 2006, Low-Frequency Asymptotic Analysis of Seismic Reflection From a Fluid-Saturated Media, *Transport in Porous Media*, Vol. 62, No. 3, p.p. 283-305.
- Goloshubin, G., VanSchuyver, C., Korneev, V., Silin, D., and Vingalov, V., 2006, Reservoir imaging using low frequencies of seismic reflections: The Leading Edge, v. 25, No 5, 527-531.
- Gennady Goloshubin and Dmitriy Silin, 2006, Frequency-dependent reflection from a permeable boundary in a fractured reservoir, 76th SEG Meeting, New Orleans.
- G. Goloshubin, D. Silin, 2006, Dual porosity Biot-Barenblatt model, 68th EAGE Meeting, Vienna.
- Zhengyun Zhou, Fred Hilterman, and Haitao Ren, 2006, Stringent assumptions necessary for pore-fluid estimation, 76th SEG Meeting, New Orleans.
- Haitao Ren, Fred Hilterman, Zhengyun Zhou, and Mike Dunn, 2006, AVO Equation without velocity and density, 76th SEG Meeting, New Orleans.
- Mingya Chen, Fred Hilterman, and Julius Doruelo, 2006, 3-D common-offset migration on a vertically aligned fracturing model, 76th SEG Meeting, New Orleans.
- Julius Doruelo, Fred Hilterman, and Gennady Goloshubin, 2006, Head waves as mechanism for azimuthal PP AVO magnitude anomalies, 76th SEG Meeting, New Orleans.

Five PhD students were working on the aspects of this project as part of their research required for the PhD degree.

The results of our activity related to this project were presented to representatives of 35 oil industry companies.

Several petroleum-related companies have joined the Reservoir Quantification Laboratory (RQL) at the University of Houston since DOE project start. The goal of RQL is similar to this DOE project. The RQL sponsors are Unocal, ExxonMobil, Devon, Geophysical Development Corporation, BP, GeoData, Apex Metalink, Paradigm, Fairfield, and Chevron. Shell and Fairfield are the industrial sponsors of this DOE project.

We were using a cooperative effort with Paradigm to assist in converting our algorithms and prototype software into their processing package FOCUS and DISCO.

REFERENCES

- Barenblatt, G.I., Zheltov, I.P., and Kochina, I.N., 1960, Basic concepts in the theory of seepage of homogeneous liquids in fissured rocks: *Journal of Applied Mathematics*, v. 24, 1286-1303.
- Biot, M.A., 1956a, Theory of propagation of elastic waves in a fluid-saturated porous solid. I. Low-frequency range: *Journal of the Acoustical Society of America*, v. 28, 168-178.
- Biot, M.A., 1956b, Theory of propagation of elastic waves in a fluid-saturated porous solid. II. Higher frequency range: *Journal of the Acoustical Society of America*, v. 28, 179-191.
- Cerveny, V. and Ravindra, R. 1971, *Theory of seismic head waves*: University of Toronto Press.
- Goloshubin, G., and Silin, D., 2006, Frequency-dependent seismic reflection from a permeable boundary in a fractured reservoir: 76th Annual International Meeting, SEG, Expanded Abstracts, 1742-1746.
- Goloshubin, G., VanSchuyver, C., Korneev, V., Silin, D., and Vingalov, V., 2006, Reservoir imaging using low frequencies of seismic reflections: *The Leading Edge*, v. 25, No 5, 527-531
- Gurevich, B., Zyrianov, V.B., and Lopatnikov, S.L., 1997, Seismic attenuation in finely layered porous rocks: Effects of fluid flow and scattering: *Geophysics*, v. 62, No 1, 319-324.
- Lynn, H.B., Simon, K.M., Bates, C.R., Van Dok, R., 1996. Azimuthal anisotropy in P-wave 3-D (multiazimuth) data: *The Leading Edge*, **15**, 923-928
- Mallat, S., 1999, *A wavelet tour of signal processing*: Academic Press, 2nd edition.
- Ruger, A., 1997. P-wave reflection coefficients for transversely isotropic models with vertical and horizontal axis of symmetry: *Geophysics*, **62**, 713-722.
- Ruger, A., and Tsvankin, I., 1997, Using AVO for fracture detection: Analytic basis and practical solutions: *The Leading Edge*, **16**, 1429–1434.
- Rutherford, S. R., and Williams, R.H., 1989, Amplitude-versus-offset in gas sands: *Geophysics*, 54, 680-688.
- Zhou, Z., Hilterman, F., Ren, H., and Kumar, M., 2005, Water-saturation estimation from seismic and rock-property trends, 75th Annual International Meeting, SEG, Expanded Abstracts, 258-261.

FUNDING

The project was selected in response to DOE's Oil and Gas Master Solicitation DE-PS-04NT15450, focus area Advanced Diagnostics and Imaging Technology.

Project Start: January 1, 2005

Project End: December 31, 2007

Anticipated DOE Total Funds: \$ 799,855.00

DOE Total Received: \$ 472,532.00

DOE Total Spent: \$ 442,773.30